European Journal of Radiology 135 (2021) 109478

Contents lists available at ScienceDirect

European Journal of Radiology

journal homepage: www.elsevier.com/locate/ejrad

Value of minimum intensity projections for chest CT in COVID-19 patients

Christian Booz [a], Thomas J. Vogl [b], U. Joseph Schoepf [c], Damiano Caruso [c,d], Maria Cristina Inserra [k], Ibrahim Yel [a], Simon S. Martin [a,c], Andreas M. Bucher [b,c], Lukas Lenga [a], Danilo Caudo [a,e], Teresa Schreckenbach [f], Niklas Schoell [g], Christian Huegel [g], Jan Stratmann [h], Mariuca Vasa-Nicotera [i], Daniel E. Rachovitsky-Duarte [j], Andrea Laghi [d], Domenico De Santis [c,d], Silvio Mazziotti [e], Tommaso D'Angelo [e,k], Moritz H. Albrecht [a,c,*]

[a] Division of Experimental Imaging, Department of Diagnostic and Interventional Radiology, University Hospital Frankfurt, Frankfurt am Main, Germany
[b] Department of Diagnostic and Interventional Radiology, University Hospital Frankfurt, Frankfurt am Main, Germany
[c] Department of Radiology and Radiological Science, Medical University of South Carolina, Charleston, USA
[d] Department of Radiological Sciences, Oncology and Pathology, Sapienzia University of Rome, Rome, Italy
[e] Department of Biomedical Sciences and Morphological and Functional Imaging, University of Messina, Messina, Italy
[f] Department of General and Visceral Surgery, University Hospital Frankfurt, Frankfurt am Main, Germany
[g] Department of Pneumonology, University Hospital Frankfurt, Frankfurt am Main, Germany
[h] Department of Hematology and Oncology, University Hospital Frankfurt, Frankfurt am Main, Germany
[i] Department of Cardiology, University Hospital Frankfurt, Frankfurt am Main, Germany
[j] Oxford Internet Institute, University of Oxford, Oxford, England, United Kingdom
[k] Department of Radiology, University Hospital Vittorio Emanuele Catania, Catania, Italy

ARTICLE INFO

Keywords:
COVID-19
Pneumonia
Viral infection
Multidetector computed tomography
Tomography
Spiral computed

ABSTRACT

Purpose: To investigate whether minimum intensity projection (MinIP) reconstructions enable more accurate depiction of pulmonary ground-glass opacity (GGO) compared to standard transverse sections and multiplanar reformat (MPR) series in patients with suspected coronavirus disease 2019 (COVID-19).

Method: In this multinational study, chest CT scans of 185 patients were retrospectively analyzed. Diagnostic accuracy, diagnostic confidence, image quality regarding the assessment of GGO, as well as subjective time-efficiency of MinIP and standard MPR series were analyzed based on the assessment of six radiologists. In addition, the suitability for COVID-19 evaluation, image quality regarding GGO and subjective time-efficiency in clinical routine was assessed by five clinicians.

Results: The reference standard revealed a total of 149 CT scans with pulmonary GGO. MinIP reconstructions yielded significantly higher sensitivity (99.9 % vs 95.6 %), specificity (95.8 % vs 86.1 %) and accuracy (99.1 % vs 93.8 %) for assessing of GGO compared with standard MPR series. MinIP reconstructions achieved significantly higher ratings by radiologists concerning diagnostic confidence (medians, 5.00 vs 4.00), image quality (medians, 4.00 vs 4.00), contrast between GGO and unaffected lung parenchyma (medians, 5.00 vs 4.00) as well as subjective time-efficiency (medians, 5.00 vs 4.00) compared with MPR-series (all $P < .001$). Clinicians preferred MinIP reconstructions for COVID-19 assessment (medians, 5.00 vs 3.00), image quality regarding GGO (medians, 5.00 vs 3.00) and subjective time-efficiency in clinical routine (medians, 5.00 vs 3.00).

Conclusions: MinIP reconstructions improve the assessment of COVID-19 in chest CT compared to standard images and may be suitable for routine application.

Abbreviations: BMI, body mass index; COVID-19, coronavirus disease 2019; GGO, ground-glass opacity; IQR, interquartile range; MinIP, minimum intensity projection; MPR, multiplanar reformat; RT-PCR, real-time reverse transcription polymerase chain reaction; SARS-CoV-2, severe acute respiratory syndrome coronavirus 2.

* Corresponding author at: University Hospital Frankfurt, Division of Experimental Imaging, Department of Diagnostic and Interventional Radiology, Theodor-Stern-Kai 7, 60590, Frankfurt am Main, Germany.
E-mail address: experimentalimaging@gmail.com (M.H. Albrecht).

https://doi.org/10.1016/j.ejrad.2020.109478
Received 25 November 2020; Accepted 10 December 2020
Available online 14 December 2020

1. Introduction

Since the pandemic of severe acute respiratory syndrome coronavirus 2 (SARS-CoV-2) and associated coronavirus disease 2019 (COVID-19) has expanded dramatically, causing 24.7 million cases with real-time reverse transcription polymerase chain reaction (RT-PCR) confirmed infection and 830,000 deaths worldwide until August 2020 [1], rapid improvements in diagnostics and therapy are necessary [2–5]. Accurate and efficient chest imaging by means of chest radiographs and computed tomography (CT) plays a key role, since pulmonary manifestation of COVID-19 in terms of viral pneumonia indicates a severe course of infection and is associated with increased morbidity and mortality [2,6,7]. Presence or absence of chest imaging findings significantly influence clinical patient management with regards to the decision to hospitalize versus home-isolate [2,6,8]. CT represents the current imaging standard for the assessment of pulmonary manifestation of COVID-19 [9–15]. Notably, several studies indicated that chest CT offers greater sensitivity for COVID-19 compared to RT-PCR [12,16,17]. This high sensitivity is mainly based on the ability to detect early infiltration of lung parenchyma as indicated by ground-glass opacity (GGO) [8,18,19]. GGO, however, can be missed on standard transverse CT reconstructions and multiplanar reformats (MPRs) in certain cases due to overlying bronchovascular structures [20–22], which may be critical because even subtle GGO commonly tend to worsen rapidly in COVID-19 patients causing the need for prompt hospitalization and oxygen therapy [18,23]. Therefore, it is crucial to detect GGO in the earliest stages in order to enable highly accurate severity assessment thereby improving clinical patient management and outcome. A few studies suggested a higher accuracy of dedicated minimum intensity projection (MinIP) reconstructions regarding CT-based assessment of GGO in comparison with standard MPRs in interstitial lung disease [21,22,24,25]. MinIP reconstructions represent a volumetric rendering technique allowing for improved visualization of low-density structures such as lung parenchyma while suppressing hyper-attenuating structures such as lung vessels. However, MinIP series are not regularly reconstructed in chest CT scans of COVID-19 patients.

Therefore, we compared MinIP reconstructions with standard MPR in chest CT scans of patients with suspected COVID-19 assessing the diagnostic accuracy, diagnostic confidence, image quality, subjective time-efficiency and general suitability in clinical routine of detecting pulmonary manifestations.

2. Material and methods

2.1. Study population

This HIPAA compliant study was approved by the institutional review boards of all participating institutions with a waiver for informed consent. Patients were enrolled at three sites in *BLINDED* (*BLINDED* [n = 77]; *BLINDED* [n = 28]) and *BLINDED* (*BLINDED* [n = 126]) for this retrospective study. Consecutive patients of 18 years of age or older, who had undergone non-contrast chest CT scans due to suspected COVID-19 within clinical routine between March and April 2020 were initially considered for inclusion (n = 231). CT scans with insufficient image quality were excluded (n = 8). All of the potentially includable CT scans were assessed by the reference standard in this study for the presence of COVID-19. CT scans with ambiguous findings were excluded (n = 16). The reference standard revealed a total of 162 CT scans positive for COVID-19 and 45 scans negative for COVID-19. From the 162 positive CT scans, 13 were tested negative by RT-PCR and were excluded. From the 45 negative CT scans, 9 were tested positive by RT-PCR and were also excluded. Finally, a total of 149 CT scans positive for COVID-19 with RT-PCR confirmed SARS-CoV-2 infection and 36 CT scans negative for COVID-19 with confirmed negative RT-PCR testing for SARS-CoV-2 were included (Fig. 1).

2.2. CT scan protcols and image reconstruction

CT scans were non-contrast single-energy CT examinations regularly performed within daily routine and with application of the departments' standard scan protocols using 120 kV tube voltage. Mean volume CT dose index was 5.3 mGy ± 1.4 (range, 2.5–7.9 mGy) and mean dose-length product was 182.4 mGy · cm ± 34.2 (range, 76.6–286.1 mGy · cm).

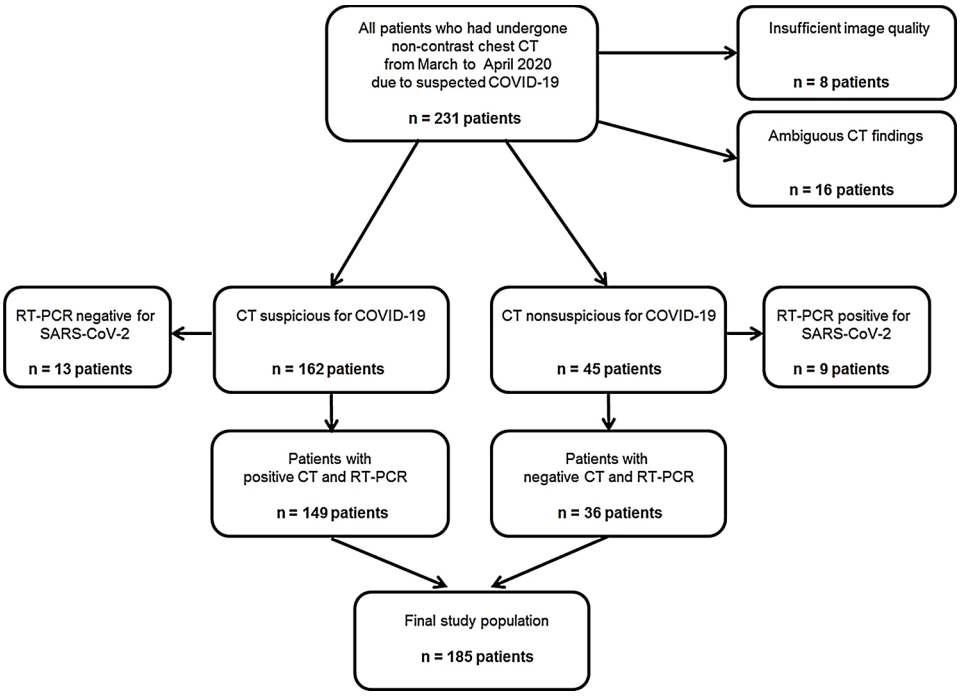

Fig. 1. Flow chart of patient inclusion. COVID-19: coronavirus disease 2019; RT-PCR: real-time reverse transcription polymerase chain reaction; SARS-CoV-2:severe acute respiratory syndrome coronavirus 2.

For image evaluation, axial and coronal MinIP series (section thickness, 3 mm; increment, 3 mm) were additionally generated besides axial and coronal MPR series for clinical routine interpretation (section thickness, 1 mm; increment, 1 mm). Both reconstruction approaches were based on dedicated lung reconstruction kernels. Section thickness and increment were determined according to the recommendations of the European Society of Thoracic Imaging [26].

2.3. Multireader analysis of GGO

All images were evaluated on a conventional PACS workstation (Centricity 4.2; GE Healthcare, Little Chalfont, UK). For definition of the reference standard, two experienced board-certified chest radiologists (*BLINDED*, and *BLINDED* with 33 and 9 years of experience in chest imaging) assessed all available CT series in consensus – reading sessions for the presence of GGO. The radiologists were instructed to not only assess CT scans for GGO presence on a per-patient level, but also on a per-lobe level. Despite GGO, other findings in COVID-19 such as consolidation, septal thickening, bronchiectasis and pleural effusion were noted. Readers were blinded to any clinical information and were permitted to adjust window settings. In addition, the amount and percentage of pulmonary opacity were quantified using semi-automatic research prototype software and standard MPR images (Frontier CT Pneumonia Analysis, Siemens Healthineers, Forchheim, Germany) by a radiologist with 5 years of experience.

Subsequently, six radiologists (*BLINDED*, board-certified radiologist with 10 years of chest imaging experience; *BLINDED*, board-certified radiologist with 9 of years of chest imaging experience; *BLINDED*, radiology resident with 6 years of chest imaging experience; *BLINDED*, radiology resident with 6 years of chest imaging experience; *BLINDED*, radiology resident with 5 years of chest imaging experience; *BLINDED*, radiology resident with 5 years of chest imaging experience), independently analyzed standard MPR series. All radiologists were blinded to clinical data and able to adjust window settings freely and to scroll through the entire stack of MPR CT series. Additionally, cases were displayed randomly. Radiologists were asked to note the presence of GGO on a per-patient and per-lobe analysis. After an interval of two weeks to avoid recall bias, the radiologists assessed randomly ordered MinIP reconstructions with the same criteria. All analyses were performed without access to clinical data. Diagnostic confidence for the detection of GGO, general image quality, contrast between GGO and unaffected lung parenchyma, and subjective time-efficiency were assessed using five-point Likert scales (1=unacceptable, 2=acceptable, 3=moderate, 4=good, and 5=excellent).

In addition, MinIP and MPR series of a randomized sample of patients with RT-PCR confirmed COVID-19 (n = 50) were shown separately in randomized order on dedicated radiological monitors for diagnosis (Eizo, Hakusan, Japan) to five clinicians (*BLINDED*, board-certified pneumologist; *BLINDED*, board-certified pneumologist; *BLINDED*, board-certified cardiologist; *BLINDED*, board-certified general surgeon; *BLINDED*, board-certified internist). The clinicians independently assessed each series for the suitability for COVID-19 assessment in general, for the image quality regarding GGO, and for subjective time-efficiency in clinical routine by application of the same five-point Likert scale.

2.4. Statistical analysis

Statistical analysis was performed using dedicated software (SPSS Statistics for Windows, version 23.0, IBM, Armonk, NY; MedCalc for Windows, Version 13, MedCalc, Mariakerke, Belgium). Mean ages were expressed as patient-level means. Normality of data patient age, image ratings) was assessed by using the Shapiro-Wilk test. Normally distributed data (patient age, body mass index [BMI]) were further analyzed with the Student *t*-test. Non-normally distributed data (image ratings by radiologists and clinicians) were compared using the Mann-Whitney-U test. A *P* value threshold less than 0.05 indicated a statistically significant difference.

Sensitivity, specificity, positive predictive and negative predictive values (PPV and NPV) and accuracy values were computed on a per-patient and per-lobe basis. Per-patient values were defined as a binary classification determined from the scores of all 6 readers for the detection of GGO. If a reader noted at least one GGO in a patient, that patient would have been labeled positive. Conversely, without detecting GGO, the patient would be negative. Clustering of lobes per patient for each reader and for consensus on the basis of a contingency table was accounted for according to the method implemented by Genders et al. [27]. Generalized estimating equations (GEE) on the basis of logistic regression analyses were applied to calculate the sensitivity and specificity of MinIP and MPR series on a lobar level within patients in order to allow for statistical comparison. In this context, radiologists were considered as independent, whereas lung lobes were interpreted as dependent within the 185 independent clusters (patients). Both radiologists and lung lobes were considered as a level of hierarchy. GEE was applied with a working correlation matrix according to Genders et al. [27]. Diagnostic accuracy parameters were compared between MinIP and MPR series by application of the McNemar test for binary matched-pairs data. Inter-reader agreement was analyzed by calculation of weighted Fleiss' κ according to Landis and Koch [28].

3. Results

3.1. Patient characteristics

A total of 185 patients (mean age, 67 ± 12; range, 19−94 years) were finally analyzed in this study. Detailed patient characteristics and known comorbidities are listed in Table 1. GGO were present in 149 patients (149/185, 80.5 %). Furthermore, the reference standard revealed consolidations in 91 patients (49.2 %), bronchiectases in 50 patients (27.0 %), septal thickening in 138 patients (74.6 %), crazy paving in 36 patients (19.5 %) and pleural effusions in 37 patients (20.0 %). Semi-automatic lung analysis using prototype software revealed a mean pulmonary volume opacity of 720.65 mL (19.4 %) in the patients positive for COVID-19 (Table 2).

3.2. Diagnostic accuracy

Regarding the assessment of GGO per patient, MinIP reconstructions showed significantly higher overall sensitivity (893/894 [99.9 %; 95 % CI, 98.5–99.9 %] vs 855/894 [95.6 %; 95 % CI, 94.2−97.0%]), specificity (207/216 [95.8 %; 95 % CI, 94.1−97.5%] vs 186/216 [86.1 %; 95

Table 1
Patient characteristics.

Characteristics	Value
Number of overall patients (women; men)	**185** (78; 107)
Overall mean age ± SD, range	**67** ± 12, 19−94
Overall mean BMI ± SD, range	**27** ± 3, 18−37
Mean age of women ± SD, range (Mean BMI of women ± SD, range)	**66** ± 13, 25−94 (26 ± 4, 18−35)
Mean age of men ± SD, range (Mean BMI of men ± SD, range)	**68** ± 14, 19−89 (28 ± 5, 19−37)
Number of patients with diabetes mellitus	**43/185** (23.2%)
Number of patients with arterial hypertension	**77/185** (41.6%)
Number of patients with coronary artery disease	**38/185** (20.5%)
Number of patients with chronic kidney disease	**30/185** (16.2%)
Number of patients with immunosuppressive therapy	**42/185** (22.7%)
Number of patients with cancer	**59/185** (31.8%)
Number of patients with asthma bronchiale	**13/185** (7.0%)
Number of patients with COPD	**32/185** (17.3%)

BMI: body mass index; COPD: chronic obstructive pulmonary disease; SD: standard deviation.

Table 2
CT findings.

Finding	Number of patients
GGO	**149/185** (80.5%)
Consolidation	**91/185** (49.2%)
Bronchiectasis	**50/185** (27.0%)
Septal thickening	**138/185** (27.0%)
Crazy paving	**56/185** (30.3%)
Pleural effusion	**37/185** (20.0%)
Mediastinal lymphadenopathy	**53/185** (28.6%)
Software-based analysis:	**Value**
Mean lung volume of opacity overall	720.7 mL (19.4%)
Mean right lung volume of opacity	483.8 mL (20.4%)
Mean left lung volume of opacity	312.0 mL (18.7%)

GGO: ground-glass opacity.

% CI, 84.1−88.2%]), PPV (893/902 [99.0 %; 95 % CI, 98.1−99.8%] vs 855/885 [96.6 %; 95 % CI, 95.298.0 %]), NPV (207/208 [99.5 %; 95 % CI, 99.2−99.9%] vs 186/225 [82.7 %; 95 % CI, 81.1−84.1%]) and accuracy (1100/1110 [99.1 %; 95 % CI, 98.3−99.8%] vs 1041/1110 [93.8 %; 95 % CI, 92.4−95.1%] compared with standard MPR series (all comparisons, $P < .001$). Results of each reader are shown in Table 3. Inter-reader agreement was excellent for MinIP reconstructions and for standard MPR series ($\kappa = 0.97$ vs $\kappa = 0.81$, $P < .001$). In four patients with early stage COVID-19, GGO was completely missed using MPR series, but detected by analyzing MinIP reconstructions in each patient by every reader in this study. In all of these patients, GGO was the only imaging finding indicative of early stage COVID-19 (RT-PCR confirmed SARS-CoV-2 infection in each case). Fig. 2 shows one of those four patients with missed GGO on a per-patient level.

The analysis per lung lobe demonstrated higher overall sensitivity (3791/3840 [98.7 %; 95 % CI, 97.5−99.7%] vs 3530/3840 [91.9 %; 95 % CI, 91.2−92.8%]), specificity (1691/1710 [98.9 %; 95 % CI, 97.9−99.9%] vs 1623/1710 [94.9 %; 95 % CI, 93.8−95.9%]), PPV (3791/3810 [99.5 %; 95 % CI, 99.2−100.0%] vs 2530/3617 [97.6 %; 95 % CI, 96.4−98.8 %]), NPV (1691/1740 [97.2 %; 95 % CI, 96.3−98.3%] vs 1623/1933 [84.0 %; 95 % CI, 82.5−85.5%]) and accuracy (5482/5550 [98.8 %; 95 % CI, 97.8−99.8%] vs 5153/5550 [92.8 %; 95 % CI, 91.5−94.3 %]) of MinIP reconstructions for assessing GGO compared with standard MPR images taking clustering into account (all comparisons, $P < .001$). Inter-reader agreement was excellent for MinIP reconstructions (κ=0.97) and for standard MPRs (κ=0.84) ($P < .001$). Table 4 shows the results of each reader. The visualization of GGO by means of MPR vs MinIP reconstructions is illustrated in Fig. 3.

3.3. Radiologists' image ratings

Subjective image rating by radiologists revealed high diagnostic confidence for the assessment of GGO by using MinIP reconstructions with a mean score of 4.59 ± 0.58 (95 % CI, 4.56–4.63) and a median of 5.00 (95 % CI, 5.00−5.00; interquartile range [IQR], 5.00−5.00; range, 2.00–5.00) compared to standard MPR series with a mean score of 4.26 ± 0.73 (95 % CI, 5.00−5.00) and a median of 4.00 (95 % CI, 4.00−4.00; IQR, 4.00−4.00; range, 2.00–5.00) ($P < .001$) (Fig. 4). Inter-reader agreement was excellent for MinIP reconstructions ($\kappa = 0.89$) and good for standard MPR images ($\kappa = 0.75$).

The image quality in MinIP reconstructions was assessed with a mean score of 4.27 ± 0.78 (95 % CI, 4.23–4.32) and a median of 4.00 (95 % CI, 4.00−4.00; IQR, 4.00−4.00; range, 2.00–5.00), whereas MPR series were rated with a mean score of 4.13 ± 0.81 (95 % CI, 4.08–4.17) and a median of 4.00 (95 % CI, 4.00−4.00; IQR, 4.00−4.00; range, 2.00–5.00), indicating a significant difference between both reconstruction algorithms ($P < .001$). Inter-reader agreement was excellent for MinIP ($\kappa = 0.89$) and standard MPR series ($\kappa = 0.88$).

Readers rated the contrast between GGO and unaffected normal lung parenchyma in MinIP reconstructions with a mean score of 4.53 ± 0.72 (95 % CI, 4.49–4.58) and a median of 5.00 (95 % CI, 5.00−5.00; IQR, 5.00−5.00; range, 2.00–5.00). MPR series were rated with a mean score of 3.86 ± 0.80 (95 % CI, 3.81–3.91) and a median of 4.00 (95 % CI, 4.00−4.00; IQR, 4.00−4.00; range, 1.00–5.00). The difference between both reconstruction types was significant ($P < .001$) (Fig. 5). Inter-

Table 3
Diagnostic accuracy for the assessment of GGO per patient.

		Sensitivity	Specificity	PPV	NPV	Accuracy
Overall	MPR	95.6 % (855/894) [94.2−97.0%]	86.1 % (186/216) [84.1−88.2%]	96.6 % (855/885) [95.2−98.0%]	82.7 % (186/225) [81.1−84.1%]	93.8 % (1041/1110) [92.4−95.1%]
	MinIP	99.9 % (893/894) [98.5−100.0%]	95.8 % (207/216) [94.1−97.5%]	99.0 % (893/902) [98.1−99.8%]	99.5 % (207/208) [99.2−99.9%]	99.1 % (1100/1110) [98.3−99.8%]
Reader 1	MPR	95.3 % (142/149) [93.1−97.4%]	94.4 % (34/36)[92.3−96.6%]	98.6 % (142/144) [97.7−99.7%]	82.9 % (34/41)[80.2−84.9%]	95.1 % (176/185) [93.2−97.4%]
	MinIP	100 % (149/149) [100.0 %]	97.2 % (35/36)[95.2−99.3%]	99.3 % (149/150) [98.4−99.9%]	100 % (35/35)[100.0 %]	99.4 % (184/185) [98.9−99.9%]
Reader 2	MPR	95.3 % (142/149) [93.1−97.4%]	88.9 % (32/36)[86.5−91.2%]	97.3 % (142/146) [95.3−99.8%]	82.1 % (32/39)[80.1−84.3%]	94.0 % (174/185) [91.2−97.0%]
	MinIPx	100 % (149/149) [100.0 %]	97.2 % (35/36)[95.2−99.3%]	99.3 % (149/150) [98.4−99.9%]	100 % (35/35)[100.0 %]	99.4 % (184/185) [98.9−99.9%]
Reader 3	MPR	95.3 % (142/149) [93.2−98.4%]	77.8 % (28/36)[75.2−81.2%]	94.7 % (142/150) [92.1−96.6%]	80.0 % (28/35)[77.3−83.1%]	91.9 % (170/185) [89.8−94.2%]
	MinIP	100 % (149/149) [100.0 %]	97.2 % (35/36)[95.2−99.3%]	99.3 % (149/150) [98.4−99.9%]	100 % (35/35)[100.0 %]	99.4 % (184/185) [98.9−99.9%]
Reader 4	MPR	96.0 % (143/149) [93.5−98.6%]	80.6 % (29/36)[77.2−83.7%]	95.3 % (143/150) [93.1−97.6%]	82.9 % (29/35)[79.3−86.1%]	92.9 % (172/185) [90.2−95.2%]
	MinIP	100 % (149/149) [100.0 %]	97.2 % (35/36)[95.2−99.3%]	99.3 % (149/150) [98.4−99.9%]	100 % (35/35)[100.0 %]	99.4 % (184/185) [98.9−99.9%]
Reader 5	MPR	95.3 % (142/149) [93.1−97.4%]	77.8 % (28/36)[73.1−81.1%]	94.7 % (142/150) [92.1−96.6%]	80.0 % (28/39)[77.1−83.3%]	91.9 % (170/185) [89.2−94.1%]
	MinIP	100 % (149/149) [100.0 %]	97.2 % (35/36)[95.2−99.3%]	99.3 % (149/150) [98.4−99.9%]	100 % (35/35)[100.0 %]	99.4 % (184/185) [98.9−99.9%]
Reader 6	MPR	96.6 % (144/149) [94.3−98.7%]	86.1 % (31/36)[84.2−88.3%]	96.6 % (144/149) [94.3−98.9%]	86.1 % (31/36)[84.2−88.3%]	94.6 % (175/185) [91.7−97.5%]
	MinIP	99.3 % (148/149) [98.8−99.8%]	88.9 % (32/36)[86.3−91.2%]	97.4 % (148/152) [95.1−99.5%]	97.0 % (32/33)[95.3−98.8%]	97.2 % (180/185) [95.1−99.2%]

Data in brackets are numerators and values in square brackets are 95 % confidence intervals. Reader 1 had 10 year of experience in chest imaging; reader 2, 9 years; reader 3, 6 years; reader 4, 6 years; reader 5, 5 years; and reader 6, 5 years.
GGO: ground-glass opacity; MinIP: minimum intensity projection; MPR: multiplanar reformat; PPV: positive predictive value; NPV: negative predictive value.

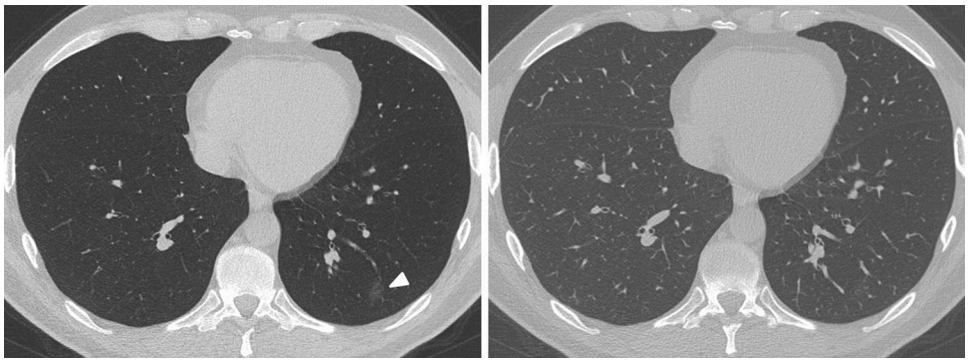

Fig. 2. A 37-years-old man, who presented to the emergency department with cough and fever. An immediate CT scan was performed due to suspected pulmonary coronavirus disease 2019 (COVID-19) manifestation. The axial minimum intensity projection (MinIP) reconstruction (left side) shows focal subtle ground-glass opacity (GGO) in the left lower lung lobe (*arrowhead*) suspicious for early stage pulmonary COVID-19, which was missed on axial multiplanar reformat (MPR) series (right side) by 6/6 readers in this study. Real-time reverse transcription polymerase chain reaction (RT-PCR) confirmed severe acute respiratory syndrome coronavirus 2 (SARS-CoV-2) infection.

Table 4
Diagnostic accuracy for the assessment of GGO per lung lobe.

		Sensitivity	Specificity	PPV	NPV	Accuracy
Overall	MPR	91.9 % (3530/3840) [91.2–92.8%]	94.9 % (1623/1710) [93.8–95.9%]	97.6 % (2530/3617) [96.4–98.8%]	84.0 % (1623/1933) [82.5–85.5%]	92.8 % (5153/5550) [91.5–94.3%]
	MinIP	98.7 % (3791/3840) [97.5–99.7%]	98.9 % (1691/1710) [97.9–99.9%]	99.5 % (3791/3810) [99.2–100.0%]	97.2 % (1691/1740) [96.3–98.3%]	98.8 % (5482/5550) [97.8–99.8%]
Reader 1	MPR	91.9 % (588/640) [90.2–93.3%]	98.6 % (281/285) [97.5–99.8%]	99.3 % (588/592) [98.8–99.9%]	84.4 % (281/333) [82.2–86.4%]	93.9 % (869/925) [92.5–95.2%]
	MinIP	99.1 % (634/640) [0.98.4–99.8%]	99.3 % (283/285) [98.9–99.9%]	99.7 % (634/636) [99.2.–100.0%]	97.9 % (283/289) [96.2–99.4%]	99.1 % (917/925) [98.4–99.9%]
Reader 2	MPR	91.4 % (585/640) [89.3–93.5%]	97.9 % (279/285) [95.6–99.3%]	99.0 % (585/591) [98.1–99.9%]	83.5 % (279/334) [81.4–85.5%]	93.4 % (864/925) [91.5–95.3%]
	MinIP	98.7 % (632/640) [97.7–99.6%]	99.3 % (283/285) [98.9–99.9%]	99.7 % (632/634) [99.4–100.0%]	97.3 % (283/291) [95.3–99.3%]	98.9 % (915/925) [98.2–99.6%]
Reader 3	MPR	91.9 % (588/640) [90.0–93.7%]]	93.7 % (267/285) [92.4–95.1%]	97.0 % (588/606) [95.9–98.1%]	83.7 % (267/319) [81.7–85.6%]	92.4 % (855/925) [91.2–94.1%]
	MinIP	98.6 % (631/640) [97.3–99.8%]	98.9 % (282/285) [97.9–99.9%]	99.5 % (631/634) [99.2–100.0%%]	96.9 % (282/291) [95.4–98.2%]	99.0 % (916/925) [98.0–99.8%]
Reader 4	MPR	92.0 % (589/640) [90.1–93.9%]	94.0 % (268/285) 92.2–95.8%]	97.2 % (589/606) [96.1–98.1%]	84.0 % (268/285) [81.8–86.4%]	92.6 % (857/925) [91.3–94.3%]
	MinIP	98.7 % (632/640) [97.7–99.6%]	99.3 % (283/285) [98.9–99.9%]	99.7 % (632/634) [99.4–100.0%]	97.3 % (283/291) [95.3–99.3%]	98.9 % (915/925) [98.2–99.6%]
Reader 5	MPR	91.4 % (585/640) [89.5–93.3%]	97.9 % (279/285) [96.8–98.9%]	99.0 % (585/591) [98.0–99.9%]	83.5 % (279/334) 81.5–85.4%]	93.4 % (864/925) [92.3–94.5%]
	MinIP	98.6 % (631/640) [97.3–99.8%]	98.9 % (282/285) [97.9–99.9%]	99.5 % (631/634) [99.2–100.0%%]	96.9 % (282/291) [95.4–98.2%]	99.0 % (916/925) [98.0–99.8%]
Reader 6	MPR	93.0 % (595/640) [92.0–94.2%]	87.4 % (249/285) [85.3–89.5%]	94.3 % (595/631) [93.1–95.5%]	84.7 % (249/294) [82.6–86.7%]	91.2 % (844/925) [90.2–92.1%]
	MinIP	98.6 % (631/640) [97.76–99.5%]	97.5 % (278/285) [95.4–99.1%]	98.9 % (631/638) [98.0–99.8%)	96.9 % (278/287) [95.0–99.0%]	98.2 % (909/925) [97.3–99.2%]

Data in brackets are numerators and values in square brackets are 95 % confidence intervals. Reader 1 had 10 year of experience in chest imaging; reader 2, 9 years; reader 3, 6 years; reader 4, 6 years; reader 5, 5 years; and reader 6, 5 years.
GGO: ground-glass opacity; MinIP: minimum intensity projection; MPR: multiplanar reformat; PPV: positive predictive value; NPV: negative predictive value.

reader agreement was excellent for MinIP ($\kappa = 0.85$) and standard MPR series ($\kappa = 0.86$).

Subjective time-efficiency was assessed with a mean score of 4.63 ± 0.58 (95 % CI, 4.60–4.67) and a median of 5.00 (95 % CI, 5.00−5.00; IQR, 5.00−5.00; range, 2.00–5.00) in MinIP reconstructions, while MPR series were rated with a mean score of 3.86 ± 0.94 (95 % CI, 3.81–3.92) and a median of 4.00 (95 % CI, 4.00−4.00; IQR, 4.00−4.00; range, 2.00–5.00), indicating a significant difference between both reconstruction algorithms ($P < .001$). Inter-reader agreement was excellent for MinIP ($\kappa = 0.84$) and standard MPR series ($\kappa = 0.82$).

3.4. Clinicians' image ratings

Regarding general suitability for routine COVID-19 assessment, clinicians rated MinIP reconstructions with a mean score of 4.51 ± 0.55 (95 % CI, 4.44–4.58) and a median of 5.00 (95 % CI, 5.00−5.00; IQR, 5.00−5.00; range, 3.00–5.00). MPR series were assessed with a mean score of 2.90 ± 0.62 (95 % CI, 2.82–2.98) and a median of 3.00 (95 % CI, 3.00−3.00; IQR, 3.00−3.00; range, 2.00–4.00), showing a significant difference between both CT reconstruction algorithms ($P < .001$) (Fig. 6). Inter-reader agreement was excellent for MinIP ($\kappa = 0.82$) and standard MPR series ($\kappa = 0.83$).

The image quality in MinIP reconstructions was rated with a mean score of 4.52 ± 0.56 (95 % CI, 4.45–4.59) and a median of 5.00 (95 % CI, 4.00–5.00; IQR, 4.00–5.00; range, 3.00–5.00), while MPR series were assessed with a mean score of 3.02 ± 0.69 (95 % CI, 2.93–3.10) and a median of 3.00 (95 % CI, 3.00−3.00; IQR, 3.00−3.00; range, 2.00–4.00). There was a significant difference between both reconstruction algorithms ($P < .001$). Inter-reader agreement was excellent for MinIP ($\kappa = 0.84$) and standard MPR series ($\kappa = 0.85$).

Clinicians considered MinIP reconstructions to be highly time-efficient as indicated by a mean score of 4.50 ± 0.58 (95 % CI, 4.42–4.57) and a median of 5.00 (95 % CI, 4.00–5.00; IQR, 4.00–5.00; range, 3.00–5.00). In contrast, the subjective time-efficiency of MPR

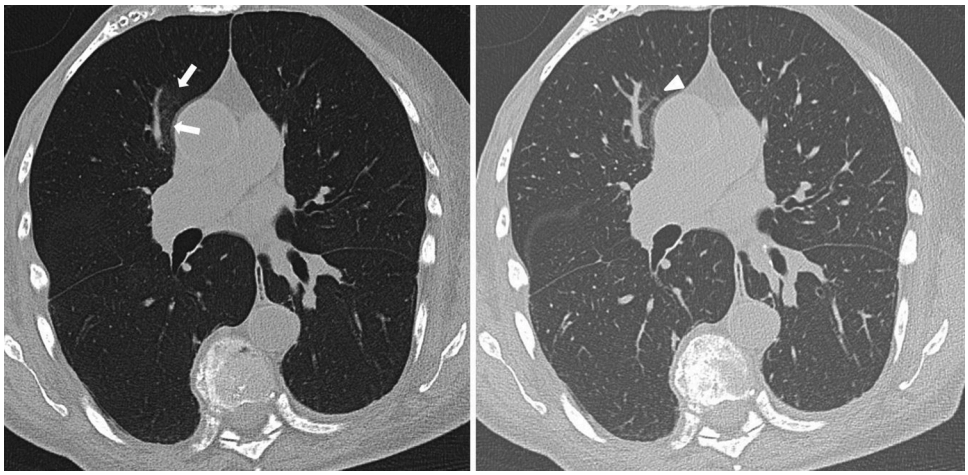

Fig. 3. A 46-years-old woman presenting to the emergency department with fever and cough. The CT scan reveals subtle ground-glass opacity (GGO) (*arrows*) in the right paramediastinal upper lung lobe suspicious for early stage coronavirus disease 2019 (COVID-19) exclusively on axial minimum intensity projection (MinIP) reconstruction (left side). On axial standard multiplanar reformat (MPR) series (right side), the GGO was missed by 3/6 readers in this study due to a masking vessel (*arrowhead*).

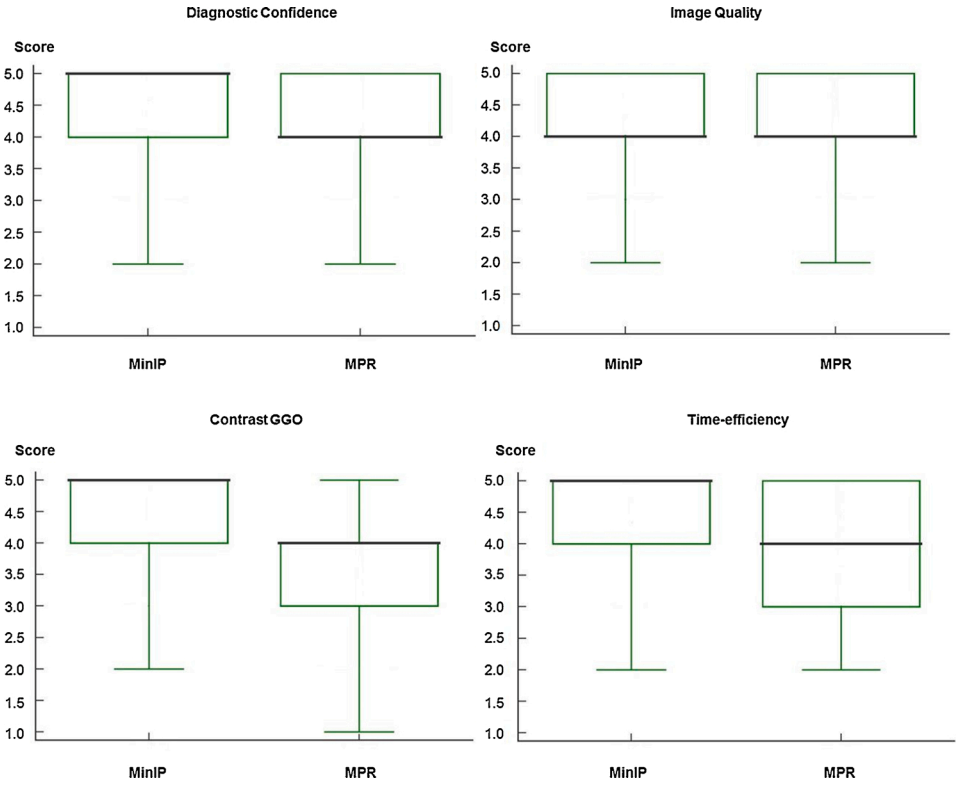

Fig. 4. Box and Whisker plots show the results of subjective image ratings by radiologists regarding the diagnostic reader confidence while assessing ground-glass opacity (GGO), general image quality, the contrast between GGO and unaffected lung parenchyma, and subjective time-efficiency of minimum intensity projection (MinIP) reconstructions and multiplanar reformat (MPR) series. Medians are displayed as horizontal bold black lines. MinIP reconstructions were rated as distinctly better than standard MPR images with regards to diagnostic confidence, contrast and subjective time-efficiency (average difference in scores, 0.33, 0.67 and 0.77, respectively, all comparisons $P < .001$), while ratings for general image quality were only slightly better for MinIP reconstructions compared to MPR series (average difference in scores, 0.14, $P < .001$).

series was rated significantly lower with a mean score of 3.00 ± 0.67 (95 % CI, 2.92–3.08) and a median of 3.00 (95 % CI, 3.00−3.00; IQR, 3.00−3.00; range, 2.00–4.00) ($P < .001$). Inter-reader agreement was excellent for MinIP reconstructions (κ = 0.86) and good for standard MPR images (κ = 0.76).

4. Discussion

We demonstrated that MinIP reconstructions significantly improve the diagnostic accuracy for assessing GGO in patients with suspected COVID-19 compared to standard MPR CT series (sensitivity, 99.9 % vs 95.6 %; specificity, 95.8 % vs 86.1 %; accuracy, 99.1 % vs 93.8 %). Diagnostic confidence, image quality, the contrast between GGO and unaffected lung parenchyma, and subjective time-efficiency were rated better for MinIP reconstructions by six radiologists (all $P < .001$). Furthermore, five clinicians preferred using MinIP reconstructions for COVID-19 assessment with regards to general suitability for clinical routine, image quality and subjective time-efficiency.

As long as control of the COVID-19 pandemic by efficient therapies and vaccination remains elusive, improvement of existing diagnostic and therapeutic means is crucial. Several studies have highlighted the substantial value of chest CT for diagnosis of GGO and subsequent triaging of COVID-19 patients – pointing out the improved diagnostic accuracy over alternative diagnostic tests such as RT-PCR [12,16,17]. The prognostic value of chest CT and its correlation with clinical parameters to monitor longitudinal course of patients with COVID-19 have also been comprehensively demonstrated [6,8,9,18]. However, the need for further refinement of chest CT in terms of COVID-19 diagnostics has been widely not met to date.

MinIP reconstructions highlight areas of low intensity such as GGO, while suppressing overlying higher attenuating structures such as bronchi or pulmonary vasculature. This fact has been also reported years

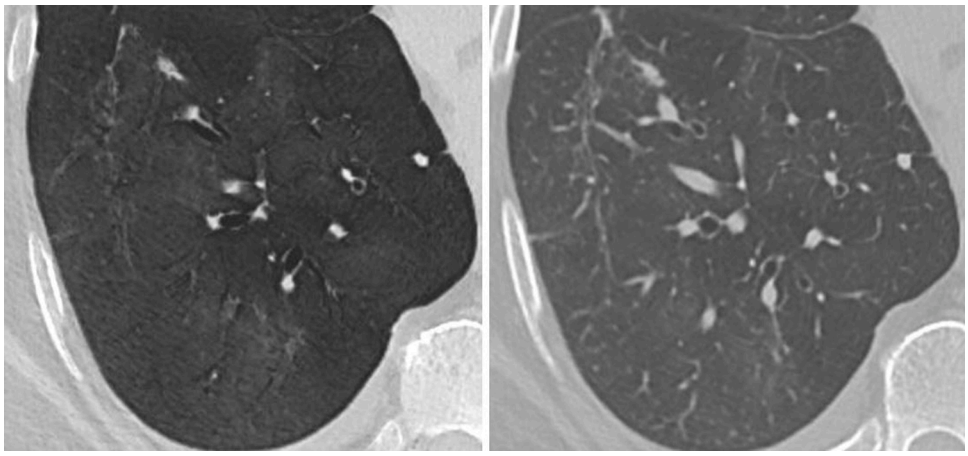

Fig. 5. CT scan of a 72-years-old man with fever, cough, shortness of breath and real-time reverse transcription polymerase chain reaction (RT-PCR) confirmed severe acute respiratory syndrome coronavirus 2 (SARS-CoV-2) infection. The axial minimum intensity projection (MinIP) reconstruction (left side) enables improved contrast between diffuse ground-glass opacity (GGO) and unaffected normal lung parenchyma in the right lower lung lobe compared to standard multiplanar reformat (MPR) series (right side).

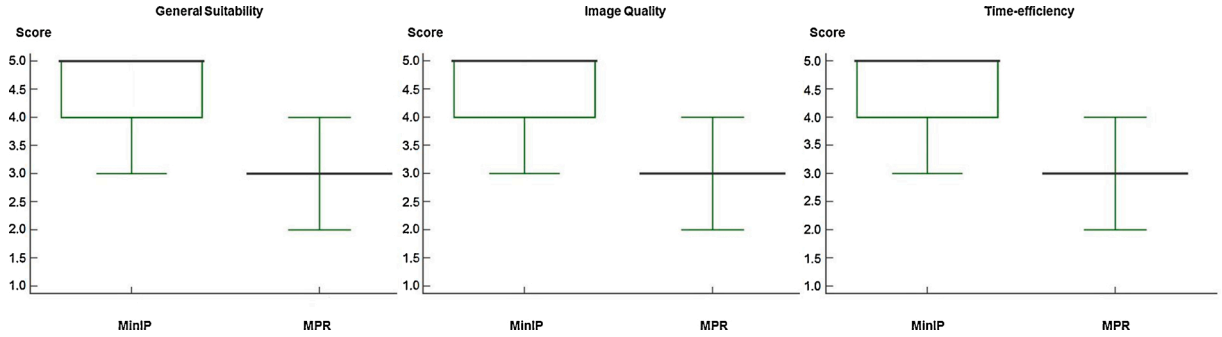

Fig. 6. Box and Whisker plots show the results of subjective image ratings by clinicians regarding the general suitability for ground-glass opacity (GGO) assessment, image quality, and subjective time-efficiency for clinical routine of minimum intensity projection (MinIP) reconstructions and multiplanar reformat (MPR) series. Medians are displayed as horizontal bold black lines. MinIP reconstructions were rated as distinctly better than standard MPR images for all categories (average difference in scores, 1.61, 1.50 and 1.50, respectively, all comparisons $P < .001$).

ago in studies on visualization of GGO due to causes other than COVID-19 [21,22,24,25]. Therefore, our results are in accordance with and effectively expand this previous evidence of facilitated detection of GGO using MinIP reconstructions. This technique appears to be suitable as an initial CT screening reconstruction algorithm in patients with suspected COVID-19 – allowing for more accurate and confident detection of GGO. In order to accomplish acceptable generalizability, our results are based on the ratings of six radiologists and five clinicians from three academic sites. The increased diagnostic accuracy and, in particular, higher sensitivity and NPV of MinIP reconstructions compared to standard MPR images in patients with suspected pulmonary COVID-19 can be considered the key result of our study. It has to be taken into account that only minor incremental diagnostic accuracy of pulmonary COVID-19 may lead to significant improvements in individual patient outcomes and facilitated hygienic workflows in busy emergency departments and hospitals in order to adhere to strict isolation guidelines. In four patients with early stage pulmonary COVID-19 manifestation and RT-PCR confirmed SARS-CoV-2 infection, GGO as the exclusive finding of pulmonary COVID-19 was completely missed by application of MPR series, but MinIP reconstructions allowed for detection of GGO in each patient by every reader in this study. In this context, there are studies demonstrating that even exclusive, subtle GGO indicating early stage COVID-19 can worsen rapidly causing the need for prompt hospitalization and oxygen therapy [18,23]. Therefore, MinIP reconstructions may substantially improve patient outcomes and facilitate triage by enabling earlier detection of pulmonary COVID-19 manifestation compared to standard CT. Furthermore, improvements in diagnostic confidence and time-efficiency may be essential in the scenario where COVID-19 admission rates rapidly soar.

Our data are supportive of a feasible and widely reproducible approach to optimize chest CT imaging of COVID-19 patients. MinIP reconstructions are usually rarely performed in clinical routine and predominantly reserved for the visualization of low-attenuation structures such as intravascular emboli, vegetations of cardiac valves, lung cysts and the assessment of the bile tree [24,29–33]. However, the approach of image reconstruction itself is simple, ubiquitously available and reproducible world-wide – independent of CT scanner technology and manufacturer. The MinIP reconstruction can be rapidly performed manually within minutes and even completed automatically. In particular, because of the increased sensitivity for pulmonary COVID-19, we propose using MinIP as a screening series when initiating chest CT analysis.

Our study has limitations beyond the retrospective study design. First, it is inherently impossible to investigate the impact of MinIP on GGO diagnostics with a dedicated reference standard in isolation, since multiple findings are found in the lung parenchyma simultaneously in the majority of COVID-19 patients. Several CT findings in COVID-19 patients have been described in the literature in addition to GGO, such as septal and bronchovascular thickening, traction bronchiectasis, consolidation and pleural effusion [10,18,19,34,35]. However, GGO is considered to represent the main finding in early pulmonary COVID-19, while most of the other criteria commonly appear in more advanced stages [8,18,19]. Therefore, the drawn conclusions may be particularly valid for patients with initial stage pulmonary COVID-19 manifestation. Second, the fact that only 19.5 % of the included patients were COVID-19 negative may limit generalizability. Third, MPR series were evaluated initially followed by image analysis of MinIP reconstructions after two weeks in all cases instead of randomizing this sequence –

possibly leading to recall bias and statistical distortion. Last, we compared different section thicknesses of MPRs and MinIPs. However, this decision was based on recommendations of the European Society of Thoracic Imaging [26].

In conclusion, we demonstrate that MinIP reconstructions can feasibly increase diagnostic accuracy for pulmonary GGO in COVID-19 while providing greater diagnostic confidence for the reader and higher subjective time-efficiency. In particular, MinIP reconstructions may facilitate early visualization and detection of initial stage pulmonary COVID-19 manifestation compared to standard CT reconstructions. Therefore, we recommend routine reconstruction of MinIP in addition to the standard workflow in CT reconstruction and analysis in patients with suspected COVID-19.

Declaration of Competing Interest

C.B. has received speaker fees from Siemens Healthineers. U.J.S. has received institutional research support, consulting fees, and/or speaker honoraria from Bayer, Bracco, Elucid BioImaging, GE, Guerbet, HeartFlow Inc., Keya Medical, and Siemens Healthineers. I.Y. has received a speaker fee from Siemens Healthineers. M.H.A. has received speaker fees from Siemens Healthineers and Bracco. The other authors have no potential conflict of interest to disclose.

References

[1] https://coronavirus.jhu.edu/map.html.
[2] Organization W.H, Coronavirus Disease 2019 (COVID-19), Situation Report, 2020, p. 51.
[3] Z.Y. Zu, M.D. Jiang, P.P. Xu, et al., Coronavirus disease 2019 (COVID-19): a perspective from China, Radiology (2020) 200490, https://doi.org/10.1148/radiol.2020200490.
[4] Guan W-j, Ni Z-y, Y. Hu, et al., Clinical characteristics of coronavirus disease 2019 in China, N. Engl. J. Med. (2020), https://doi.org/10.1001/jamanetworkopen.2020.5619.
[5] T.M. McMichael, D.W. Currie, S. Clark, et al., Epidemiology of Covid-19 in a long-term care facility in King County, Washington, N. Engl. J. Med. (2020), https://doi.org/10.1056/nejmoa2005412.
[6] Z. Wu, J.M. McGoogan, Characteristics of and important lessons from the coronavirus disease 2019 (COVID-19) outbreak in China: summary of a report of 72 314 cases from the Chinese Center for Disease Control and Prevention, JAMA (2020), https://doi.org/10.1001/jama.2020.2648.
[7] N. Goyal, M. Chung, A. Bernheim, et al., Computed tomography features of coronavirus disease 2019 (COVID-19): a review for radiologists, J. Thorac. Imaging (2020), https://doi.org/10.1097/rti.0000000000000527.
[8] W. Zhao, Z. Zhong, X. Xie, et al., Relation between chest CT findings and clinical conditions of coronavirus disease (COVID-19) pneumonia: a multicenter study, Am. J. Roentgenol. (2020) 1–6, https://doi.org/10.2214/ajr.20.22976.
[9] A. Bernheim, X. Mei, M. Huang, et al., Chest CT findings in coronavirus disease-19 (COVID-19): relationship to duration of infection, Radiology (2020) 200463, https://doi.org/10.1148/radiol.2020200463.
[10] W. Kong, P.P. Agarwal, Chest imaging appearance of COVID-19 infection, Radiol. Cardiothoracic Imaging 2 (2020), e200028, https://doi.org/10.1148/ryct.2020200028.
[11] T. Ai, Z. Yang, H. Hou, et al., Correlation of chest CT and RT-PCR testing in coronavirus disease 2019 (COVID-19) in China: a report of 1014 cases, Radiology (2020) 200642, https://doi.org/10.1148/radiol.2020200642.
[12] Y. Fang, H. Zhang, J. Xie, et al., Sensitivity of chest CT for COVID-19: comparison to RT-PCR, Radiology (2020) 200432, https://doi.org/10.1148/radiol.2020200432.
[13] H. Choi, X. Qi, S.H. Yoon, et al., Extension of coronavirus disease 2019 (COVID-19) on chest CT and implications for chest radiograph interpretation, Radiol. Cardiothoracic Imaging 2 (2020), e200107, https://doi.org/10.1148/ryct.2020200107.
[14] M. Lang, A. Som, D.P. Mendoza, et al., Detection of unsuspected coronavirus disease 2019 cases by computed tomography and retrospective implementation of the radiological society of north America/Society of thoracic Radiology/American college of radiology consensus guidelines, J. Thorac. Imaging (2020), https://doi.org/10.1097/rti.0000000000000542.
[15] S. Salehi, A. Abedi, A.R. Radmard, et al., Chest computed tomography manifestation of coronavirus disease 2019 (COVID-19) in patients with cardiothoracic conditions, J. Thorac. Imaging 35 (2020) 90–96, https://doi.org/10.1097/rti.0000000000000531.
[16] J. Xu, R. Wu, H. Huang, et al., Computed tomographic imaging of 3 patients with coronavirus disease 2019 pneumonia with negative virus real-time reverse-transcription polymerase chain reaction test, Clin. Infect. Dis. (2020), https://doi.org/10.1093/cid/ciaa207.
[17] X. Xie, Z. Zhong, W. Zhao, et al., Chest CT for typical 2019-nCoV pneumonia: relationship to negative RT-PCR testing, Radiology (2020) 200343, https://doi.org/10.1148/radiol.2020200343.
[18] Y. Wang, C. Dong, Y. Hu, et al., Temporal changes of CT findings in 90 patients with COVID-19 pneumonia: a longitudinal study, Radiology (2020) 200843, https://doi.org/10.1148/radiol.2020200843.
[19] F. Pan, T. Ye, P. Sun, et al., Time course of lung changes on chest CT during recovery from 2019 novel coronavirus (COVID-19) pneumonia, Radiology (2020) 200370, https://doi.org/10.1148/radiol.2020200370.
[20] S. Perandini, N. Faccioli, A. Zaccarella, et al., The diagnostic contribution of CT volumetric rendering techniques in routine practice, Indian J. Radiol. Imaging 20 (2010) 92, https://doi.org/10.4103/0971-3026.63043.
[21] A. Lacout, P.Y. Marcy, T.M. Ngo, et al., Multidetector row CT scan in hypersensitivity pneumonitis: contribution of minimum intensity projection reformation, J. Med. Imaging Radiat. Oncol. 55 (2011) 291–295, https://doi.org/10.1111/j.1754-9485.2011.02267.x.
[22] M. Bhalla, D.P. Naidich, G. McGuinness, et al., Diffuse lung disease: assessment with helical CT–preliminary observations of the role of maximum and minimum intensity projection images, Radiology 200 (1996) 341–347, https://doi.org/10.1148/radiology.200.2.8685323.
[23] J. Wang, J. Liu, Y. Wang, et al., Dynamic changes of chest CT imaging in patients with corona virus disease-19 (COVID-19), Zhejiang da xue xue bao Yi xue ban= J. Zhejiang Univ. Med. Sci. 49 (2020) 0, https://doi.org/10.1101/2020.06.04.20119206.
[24] Y.Y. Sabri, I.M.H. Ibrahim, S.M.T. Gamal, et al., Multi-detector CT (MDCT) evaluation in interstitial lung disease (ILD): comparison of MinIP and volumetric high resolution CT (HRCT) images, Egypt. J. Radiol. Nucl. Med. 48 (2017) 87–95, https://doi.org/10.1016/j.ejrnm.2016.11.009.
[25] C. Beigelman-Aubry, C. Hill, A. Guibal, et al., Multi–detector row Ct and postprocessing techniques in the assessment of diffuse lung disease, Radiographics 25 (2005) 1639–1652, https://doi.org/10.1148/rg.256055037.
[26] H. Prosch, C.M. Schaefer-Prokop, E. Eisenhuber, et al., CT protocols in interstitial lung diseases—a survey among members of the European Society of Thoracic Imaging and a review of the literature, Eur. Radiol. 23 (2013) 1553–1563, https://doi.org/10.1007/s00330-012-2733-6.
[27] T.S. Genders, S. Spronk, T. Stijnen, et al., Methods for calculating sensitivity and specificity of clustered data: a tutorial, Radiology 265 (2012) 910–916, https://doi.org/10.1148/radiol.12120509.
[28] J.R. Landis, G.G. Koch, The measurement of observer agreement for categorical data, Biometrics (1977) 159–174, https://doi.org/10.2307/2529310.
[29] T. Bartalena, D. Oboldi, P.L. Guidalotti, et al., Lung perfusion in patients with pulmonary hypertension: comparison between MDCT pulmonary angiography with minIP reconstructions and 99mTc-MAA perfusion scan, Invest. Radiol. 43 (2008) 368–373, https://doi.org/10.1097/rli.0b013e31816901e2.
[30] T. Smith, S. Gurudevan, V. Cheng, et al., Assessment of the morphological features of degenerative mitral valve disease using 64-slice multi detector computed tomography, J. Cardiovasc. Comput. Tomogr. 6 (2012) 415–421, https://doi.org/10.1016/j.jcct.2012.10.004.
[31] D.D. Cody, AAPM/RSNA physics tutorial for residents: topics in CT: image processing in CT, Radiographics 22 (2002) 1255–1268, https://doi.org/10.1148/radiographics.22.5.g02se041255.
[32] T. Denecke, E. Degutyte, L. Stelter, et al., Minimum intensity projections of the biliary system using 16-channel multidetector computed tomography in patients with biliary obstruction: comparison with MRCP, Eur. Radiol. 16 (2006) 1719, https://doi.org/10.1007/s00330-006-0172-y.
[33] H. Kim, S. Park, S. Park, et al., Three-dimensional reconstructed images using multidetector computed tomography in evaluation of the biliary tract, AbdominalImaging 29 (2004) 472–478, https://doi.org/10.1007/s00261-003-0123-x.
[34] F. Kay, S. Abbara, The many faces of COVID-19: spectrum of imaging manifestations, Radiol. Soc. North Am. (2020), https://doi.org/10.1148/ryct.2020200037.
[35] H. Shi, X. Han, N. Jiang, et al., Radiological findings from 81 patients with COVID-19 pneumonia in Wuhan, China: a descriptive study, Lancet Infect. Dis. (2020), https://doi.org/10.1016/s1473-3099(20)30086-4.